LOW-FREQUENCY WIND WAVE PENETRATION IN A TIDAL INLET SYSTEM DURING A SEVERE WINTER STORM

Gerbrant van Vledder[1,2)], Jeroen Adema[1)], Olger Koop[1)], François Enet[1)], and André van der Westhuysen[3)]

[1)]Alkyon Hydraulic Consultancy & Research, P.O. Box 248, 8300 AE, Emmeloord, The Netherlands.
[2)] Delft University of Technology, P.O. Box 5048, 2600 GA, Delft, The Netherlands
[3)] Deltares | Delft Hydraulics, P.O. Box 177, 2600 MH, Delft, The Netherlands

INTRODUCTION

On 9 November 2007 a severe winter storm occurred in the southern North Sea. This storm led to high water level and wave conditions along the Dutch coast. In addition it caused a significant amount of wave penetration into the Wadden Sea, a tidal basin partly sheltered from the North Sea by barrier islands. Wind, wave, bathymetric and water level data are routinely collected since 2003 in a monitoring program of Rijkswaterstaat (Zijderveld and Peters, 2008). Wave measurements are carried out in two representative tidal inlets. The first is the tidal inlet of Ameland, which is well sheltered by a large ebb-tidal delta. The second is the Dutch Eastern Wadden Sea near the Ems estuary and which is more exposed to North Sea waves. Figure 1 gives an overview of these measurement locations in the Dutch Wadden Sea. The November 2007 storm was hindcast with the SWAN model (Booij et al., 1999) in the framework of the Dutch research program SBW Waddenzee. This program aims at improving the SWAN wave model which will play a key role in the determination of Hydraulic Boundary Conditions (HBC) of the dikes along the Wadden Sea coast (Groeneweg et al., 2008).

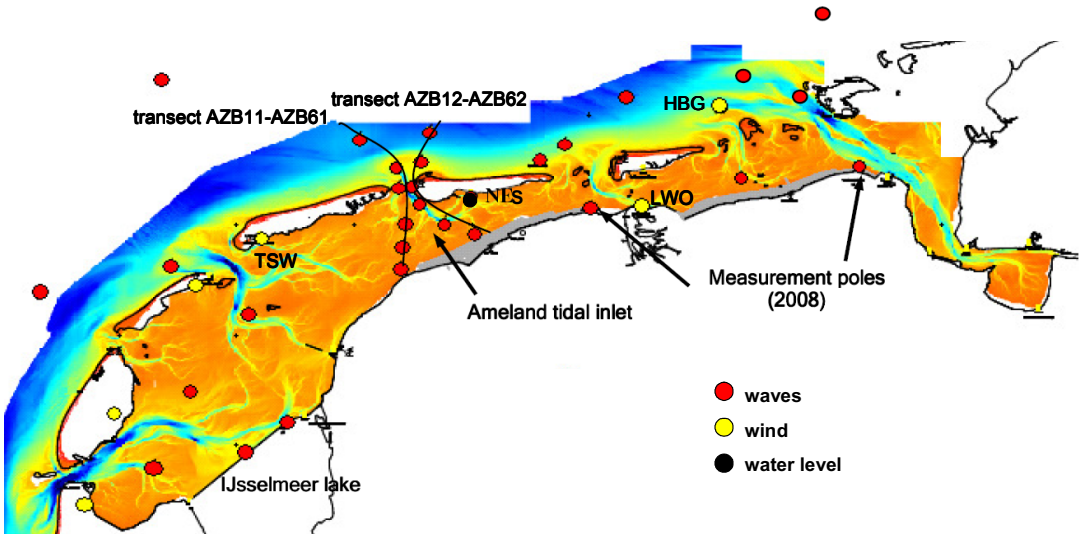

Figure 1: Situation sketch of the Dutch Wadden Sea and measurement locations (Groeneweg et al., 2008).

Various hindcast studies indicated that the tidal inlets connecting the North Sea with the Wadden Sea effectively filter most of the North Sea waves, such that the wave conditions in the Wadden Sea are mainly locally determined (Van Vledder et al., 2007, 2008). The main mechanisms responsible for this filtering are refraction and dissipation. As the waves propagate through the

tidal inlets they are refracted to the sides of the tidal channels where they dissipate on the bordering shallow tidal flats.

The storm of 9 November 2007 was hindcast with the SWAN model on a dedicated grid for the Dutch Eastern Wadden Sea. The outline of this grid and its bathymetry are shown in Figure 2. During this storm, waves were measured using six directional Waverider buoys. Three buoys, SON, WEW1 and WEO1 were located along the boundary of the computational grid, whereas the buoys UHW1, PBW1 and WRW1 were located on the shallow tidal flats in the interior of the Dutch Eastern Wadden Sea. Wind measurements were performed at various stations in the Wadden Sea of which those of station Huibertgat were used in this study.

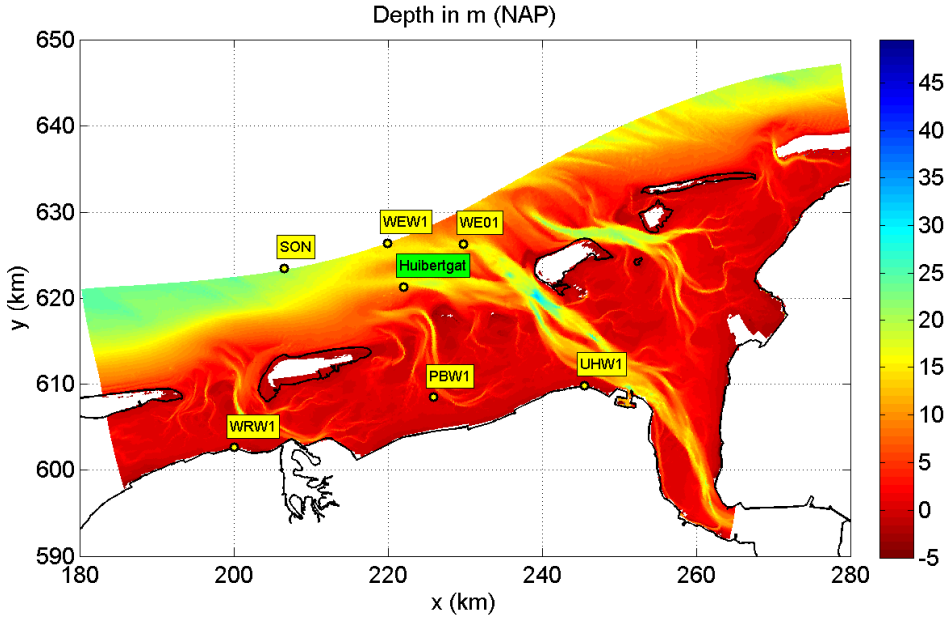

Figure 2: Outline and bathymetry of the computational grid for the Dutch Eastern Wadden Sea. Buoy locations are indicated with yellow labels, and Huibertgat with a green label.

The SWAN hindcast of the storm of 9 November 2007 showed that SWAN strongly under-predicts the amount of low-frequency wave energy at the shallow water locations in the Wadden Sea. Figure 3 shows an example of this under-prediction at three buoy locations in the eastern Wadden Sea at the high water peak of the storm. The under-estimation of low-frequency wave components by the SWAN model was also noted by Kaiser and Niemeyer (2001) in a hindcast study for the tidal inlet of Norderney in the German Wadden Sea region. Since low-frequency wave components can have significant effects on dike loads, it is crucial to remedy this short-coming of the SWAN model before it can be used in determining the HBC.

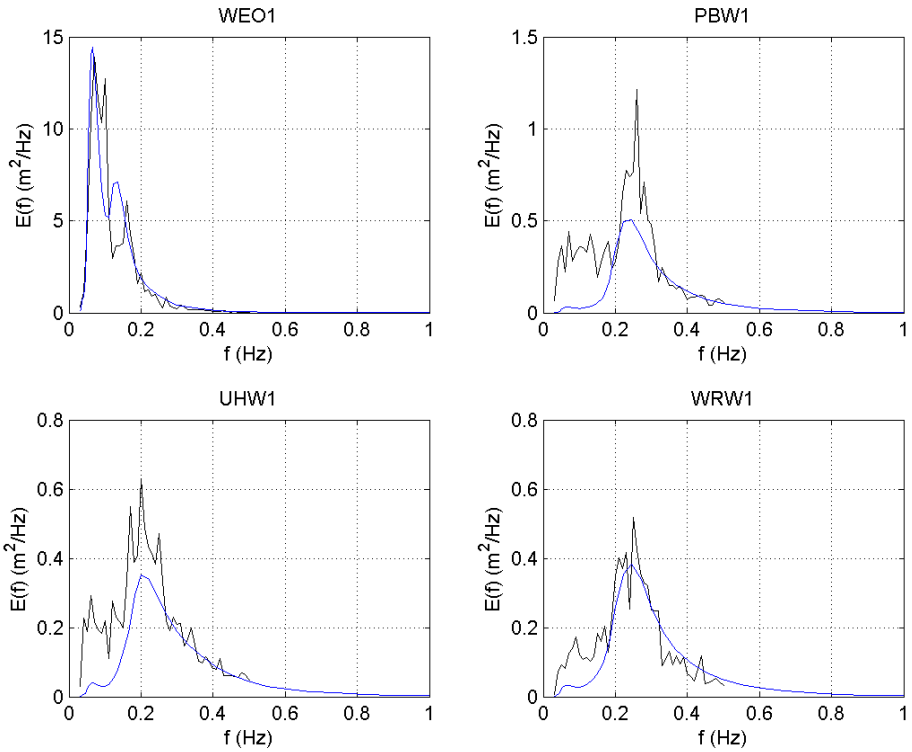

Figure 3: Measured (black lines) and computed spectra (blue lines) at four buoy locations in the Dutch Eastern Wadden Sea at storm instant 9 Nov. 2007, 9:40 hours.

This strong under-prediction of low-frequency wind wave energy motivated us to perform a detailed study into the causes of and possible solutions for this under-prediction by SWAN. An important aspect of the hindcast study was to reconstruct the time- and spatial varying current and water level fields. This was achieved using coupled flow-wave model runs on a curvi-linear computational grid for the Dutch Eastern Wadden Sea. Subsequently, a detailed wave hindcast was performed on a finer computational grid using the reconstructed current- and water level fields as input. The emphasis in the analysis of the detailed wave hindcast was on the penetration of low-frequency wave energy into the interior of the Wadden Sea. This analysis included performing sensitivity runs to determine the effect of various alternative boundary conditions and model formulations on the amount of low-frequency wave energy penetrating into the Wadden Sea.

The storm of 9 November 2007

The storm of 9 November 2007 was a dominantly NNW event. The peak of the storm, related to the maximum registered wind speed was U_{10} = 22.2 m/s and occurred at 11:00 am, whereas high water was at 10:00 am. Wind directions changed from 280º at the beginning of the storm to 320º at the end of the storm. Figure 4 shows the variation of wind speed and wind direction at four stations in the Wadden Sea. The black lines indicate the date and time of the five selected storm instants for the analysis.

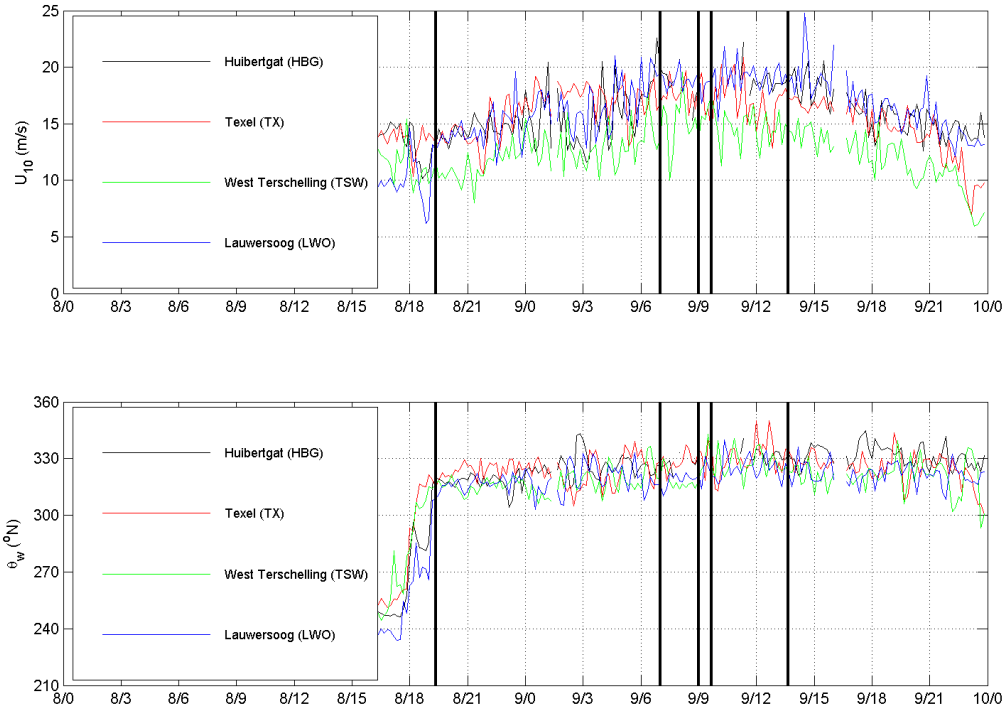

Figure 4: Time variation of wind speed and direction at four locations in the Dutch Wadden Sea during the November 2007 storm. Selected time instants are indicated with black vertical lines.

Based on water level registrations at Delfzijl, the return period of the storm is about ten years, making it a significant storm event. The offshore wave height at station SON has a maximum of H_{m0} = 8.4 m. This is close to the value H_{m0} = 8.59 m, which corresponds to a storm with a return period of 100 years[1] (WL, 2004). Therefore, this storm can be considered as a major storm of significant interest for the wave conditions at the mainland dikes. The variation of the water level h, significant wave height H_{m0} and spectral period $T_{m-1,0}$ at the measuring stations is shown in Figure 5. The peak water levels increase as the measurement station is more to the east, with the highest water level close to 5 m at station Nieuwe Statenzijl located in the eastern corner of Ems-Dollard estuary. The highest offshore wave conditions occurred at the stations SON and WEW1 with significant wave heights H_{m0} close to 8 m and spectral periods $T_{m-1,0}$ close to 14 s. The wave heights measured at buoy WEO1 are much smaller due to dissipative effects in the ebb-tidal delta. The lowest wave heights were measured at the shallow water buoys PBW1, UHW1 and WRW1. For these buoys, the wave conditions are strongly modulated by the water level. The buoys UHW1 and WRW1 even fall dry for a short period of time in the early morning and late afternoon of 9 November 2007. For buoy UHW1 the spectral period $T_{m-1,0}$ has suspiciously high values at moments with small water depths, occurring just before and after it falls dry. This is probably related to the buoy hitting the ground causing relatively long-period oscillations. Evidently, these measurements were omitted from our hindcast.

[1] Based on a Weibull fit on measured wave heights at SON over a period of 23 years.

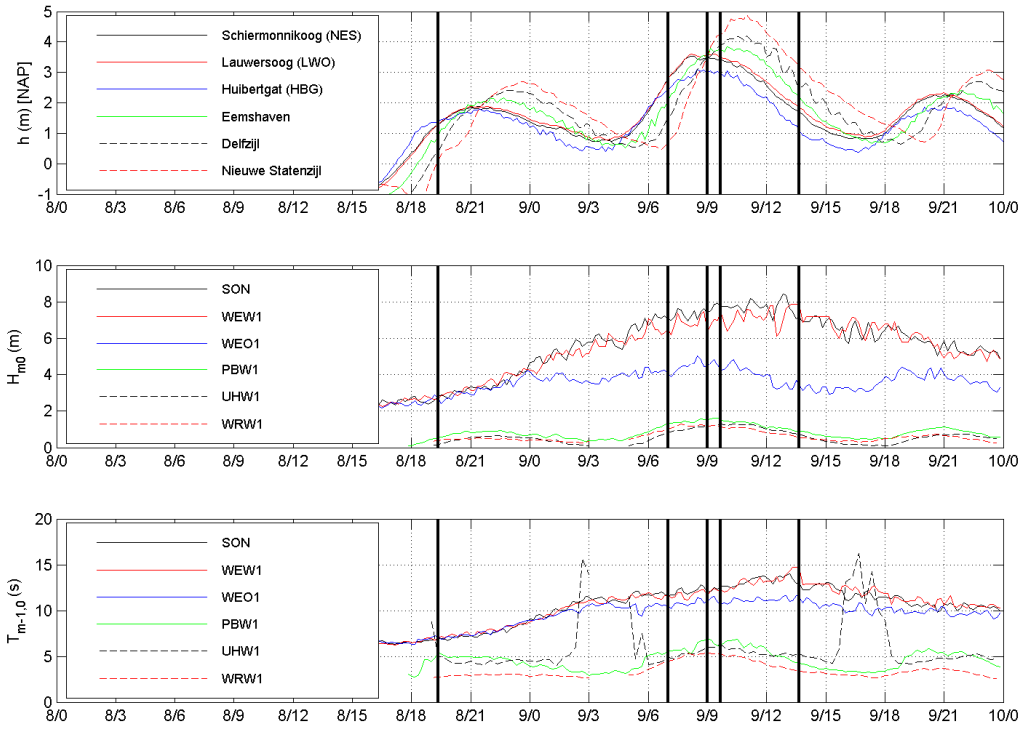

Figure 5: Time variation of water level, significant wave height H_{m0} and spectral period $T_{m-1,0}$ at the measuring stations in the Dutch Eastern Wadden Sea. Selected time instants are indicated with black vertical lines.

Reconstruction of current and water level fields

For any shallow water wave hindcast accurate current and water level fields are indispensable, especially in depth-limited situations, as shallow water effects significantly affect the waves. For the hindcast of the 9 November 2007 storm, the hydro-dynamic conditions were reconstructed using the coupled Delft3D and SWAN wave modeling system of Deltares, the Netherlands. Various modeling choices had to be made to obtain satisfactorily results, of which the type of wind forcing and the type of coupling between the flow- and the wave model were the most important. As no current velocity measurements were available for this storm, computational results were assessed on the basis of a comparison of the computed and observed water levels at six stations within the modeled area.

The coupled computations were performed on a curvi-linear grid covering the Dutch Eastern Wadden Sea. Figure 6 shows the outline of this grid, of which every third grid line is shown, together with the buoy locations. The grid cells in the lower-right corner of this grid cover the river Ems and are needed to ensure proper water storage area characteristics.

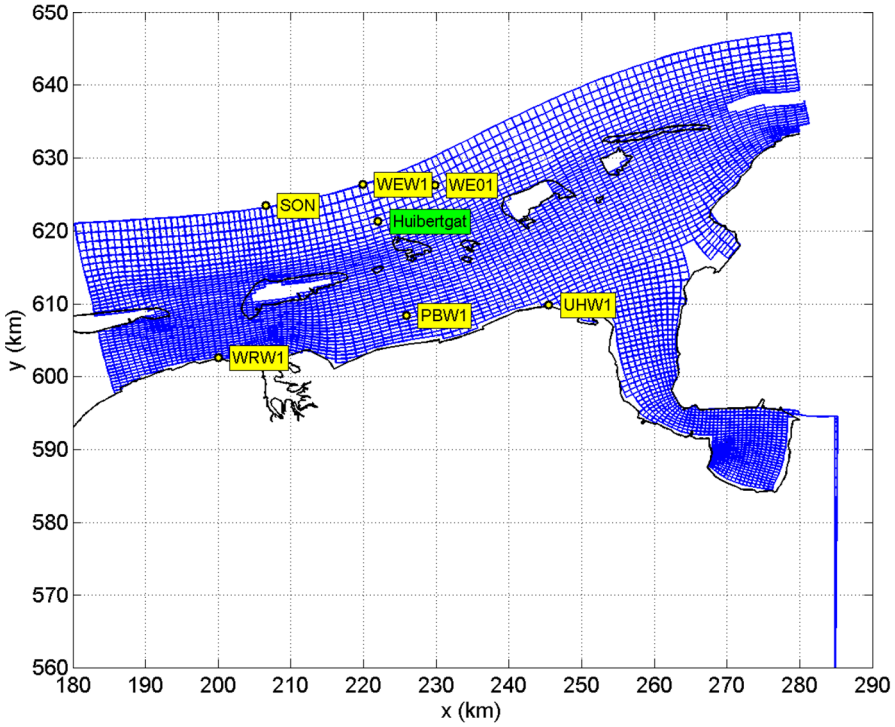

Figure 6: Computational grid for the coupled Delft3D-SWAN computations (every third grid line is shown, buoy locations (yellow labels) and wind measurement station (green label).

The flow- and wave models are driven by time varying wind fields. Usually, this is achieved using HIRLAM wind and pressure fields. These were provided every 3 hours on an 11 x 11 km grid. Data comparison against measured winds showed that the HIRLAM wind speeds did not always compare very well with the measured wind speeds. This finding led us to investigate the option using time-varying but spatially uniform wind fields based on measured winds obtained at station Huibertgat with a time step of 10 min. We chose this station because it is well exposed and located in the centre of our area of interest (See Figure 6). We assumed these winds to be representative for the Dutch Eastern Wadden Sea. A drawback of this approach is that we miss the spatial variation of the wind fields, which is inherently present in the HIRLAM fields. An advantage of our approach is that the temporal variability is better captured using measured winds than winds from the HIRLAM model. Next, we compared simulated water levels using both types of wind fields with the measured water levels in the Dutch Eastern Wadden Sea. In general we found better agreement using the uniform wind fields than using the HIRLAM wind fields. Evidently, the lack of spatial variation in our wind fields, was less important than the time variation of the wind fields.

In coastal areas like the Wadden Sea, the effects of waves on the currents and water levels can not always be neglected. We therefore performed coupled flow- wave model runs using the Delft3D-SWAN modeling system. The SWAN wave model was driven by the same uniform wind fields and applied on the same computational grid as the Delft3D model. The wave boundary conditions of the SWAN model were obtained from the wave buoys SON and WEW1 located near the northern boundary of the computational grid shown in Figure 6. The measured conditions at buoy location SON were imposed on the boundary west of location SON. The measured conditions at buoy location WEW1 were imposed on the boundary east of location WEW1. Between the

locations SON and WEW1, the boundary conditions, in terms of integral wave parameters, were linearly varying between the values imposed at the buoys locations SON and WEW1.

The flow model was run with a time step of 6 seconds. Every 10 minutes, a stationary SWAN simulation was run using the computed water level and velocity fields at that moment. The computed radiation stresses were transferred back to the flow model to include the wave effect for the following 10 minutes. The coupling interval was equal to the time step of available wind and wave data.

While testing our coupled model setup, we found that the wave conditions of WEW1 were not physically realistic along the shallow model boundary east of buoy WEW1. Since the water depth along the eastern part of the offshore model boundary was smaller than the depth at buoy WEW1, the incident wave heights were over-estimated, resulting in instabilities in our coupled model runs. A pragmatic solution was to limit the incident significant wave height to 40% of the local (time varying) water depth.

For the coupled flow-wave computations, the forces due to the waves were based on radiations stresses, and not on energy dissipation as suggested by Dingemans et al. (1987). The latter induced irregular velocity fields in the flow simulations and unexpected wave heights and dissipation pattern in the SWAN computations. As a result, unrealistic water levels were found with this type of forcing. Forcing based on radiations stresses produced realistic flow patterns and the computed water levels agreed better with observations than those based on model simulations using energy dissipation.

The results of our coupled flow-wave computations for station Lauwersoog are compared with the observed water levels in Figure 7, together with the results using a simulation run without wave effects. The difference due to wave effects is also shown. The results clearly show that inclusion of wave effects improves the accuracy of the predicted water levels considerably. For the present storm, they are responsible for about 0.4 m additional water level at the nearshore location Lauwersoog. Similar values are also found for other locations in the area of interest.

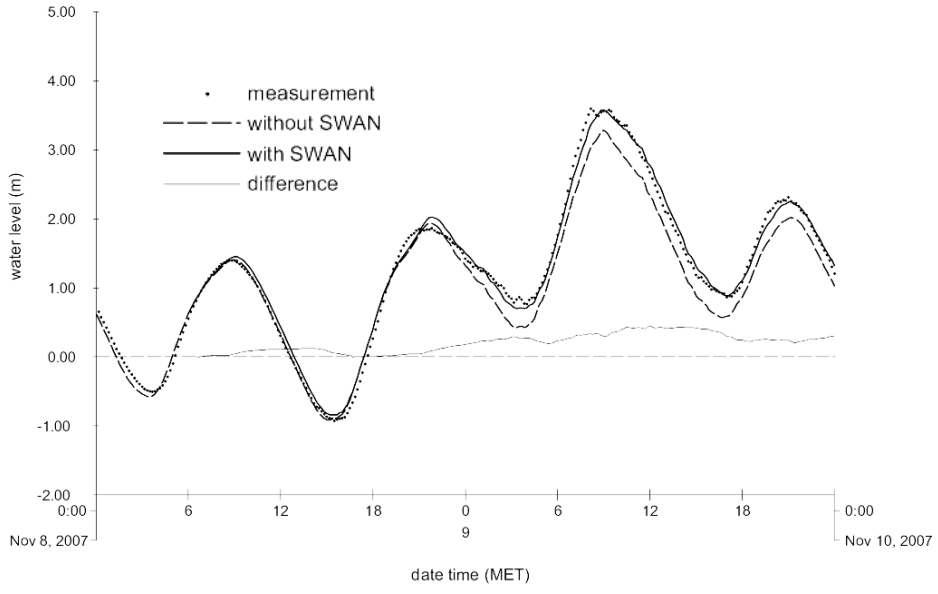

Figure 7: Comparison of measured and predicted water levels at station Lauwersoog

Detailed wave hindcast

The coupled flow-wave computations were performed on a relatively coarse computational grid. That grid was considered to be sufficiently fine to reconstruct realistic current and water level fields in the Dutch Eastern Wadden Sea for the 9 November 2007 storm, but insufficiently fine for the detailed wave hindcast. We therefore refined the computational flow-wave grid with a factor two in both grid directions for the wave model computations. In addition, detailed rectangular 3 x 3 km grids with a spatial resolution of 20 m were constructed around the shallow water buoys UHW1, PBW1 and WRW1. The computed current and water level fields, obtained in the previous activity, were interpolated to these finer grids. Bathymetric information, available on a 20 x 20 m spatial resolution, was also interpolated to these detailed grids. The detailed wave computations were performed for 5 storm instants, shown in the Figures 4 and 5. We were interested in the following situations:

- shallow water conditions, such that waves are depth-limited;
- strong tidal currents;
- penetration of low-frequency waves into the Wadden Sea.

Based on these criteria the following stationary storm instants were selected:

Storm instant	Date and time
1	8 Nov. 2007, 19:20
2	9 Nov. 2007, 07:00
3	9 Nov. 2007, 09:00
4	9 Nov. 2007, 09:40
5	9 Nov. 2007, 13:40

Table 1: Date and time of selected storm instants.

The default SWAN model settings applied here include the saturation based white-capping dissipation according to Van der Westhuysen et al. (2007) using B_r=1.75x10^{-3}, wind input according to Yan (1987), four-wave interaction using the Discrete Interaction Approximation (DIA) of Hasselmann et al. (1985), the lumped triad interaction approximation (LTA) of Eldeberky (1996) using α_{EB}=0.05 and CUTFR=2.5, surf breaking according to the Battjes-Janssen formulation (1978) using α_{BJ}=1.0 and γ_{BJ}=0.73 and the JONSWAP bottom friction formulation using $C_{f,JON}$=0.067 m^{2}s^{-3}, i.e. the recommended value for fully-growth wave spectra in shallow water (Bouws and Komen, 1983). These settings are referred to as the default model settings in the remainder.

As shown in Figure 3 the largest model errors are made for the frequency range up to 0.2 Hz. We therefore defined a low-frequency wave height H_{20} as the significant wave height based on all frequencies up to 0.2 Hz. Similarly, we defined a low-frequency spectral period T_{20}, equivalent to the spectral period $T_{m-1,0}$. The definitions of both parameters are given in Eq. (1).

$$H_{20} = 4\sqrt{\int_0^{0.2} E(f)\,df}$$
$$T_{20} = \int_0^{0.2} \frac{1}{f} E(f)\,df \Big/ \int_0^{0.2} E(f)\,df \qquad (1)$$

Figure 8 shows the geographical variation of the low-frequency wave height H_{20} in the Ducth Eastern Wadden Sea, together with the buoy locations and the bottom contours at 5 m, 10 m and

20 m water depth. It can be seen that the low-frequency wave energy hardly penetrates into the Wadden Sea. Most of this energy disappears in the tidal inlets between the Wadden islands. Some 'tongues' of low-frequency wave energy can be seen on the tidal flat about 8 km north of buoy WRW1 and on the shallow ridge in the main tidal channel about 5 km north of buoy UHW1 (see Figure 2 for the local bathymetry). The latter phenomenon is an indication that refraction directs wave energy from the tidal channels towards their neighboring shallow areas.

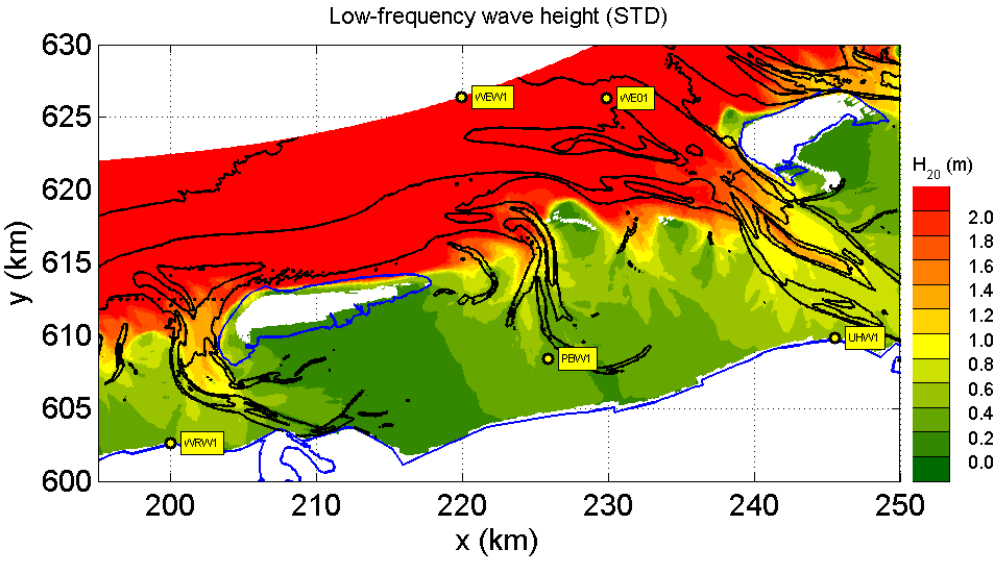

Figure 8: Geographical variation of the low-frequency wave height H_{20} in the Dutch Eastern Wadden Sea for storm instant 9 Nov. 2007, 9:40 hours using the default settings of SWAN.

The locations where refraction effects play a dominant role in the propagation of low-frequency wave energy are illustrated in Figure 9. Here, the normalized magnitude $M_{c\theta}$ of the refraction term has been obtained by integrating the spectral velocity c_θ, weighted with the action density, over the frequency range up to 0.20 Hz. The normalization was carried out by dividing with the total wave variance over the same frequency range. The magnitude of the refraction term has been computed as:

$$M_{c,\theta} = \int_0^{2\pi} \int_0^{0.2} \left\{ \left| \frac{\partial c_\theta N}{\partial \theta} \right| \right\} df \, d\theta \qquad (2)$$

The geographical variation of the normalized magnitude of the refraction term reflects the pattern of the tidal channels, especially along their shoulders. A similar analysis was carried out by Holthuijsen et al. (2008) for the tidal inlet of Ameland.

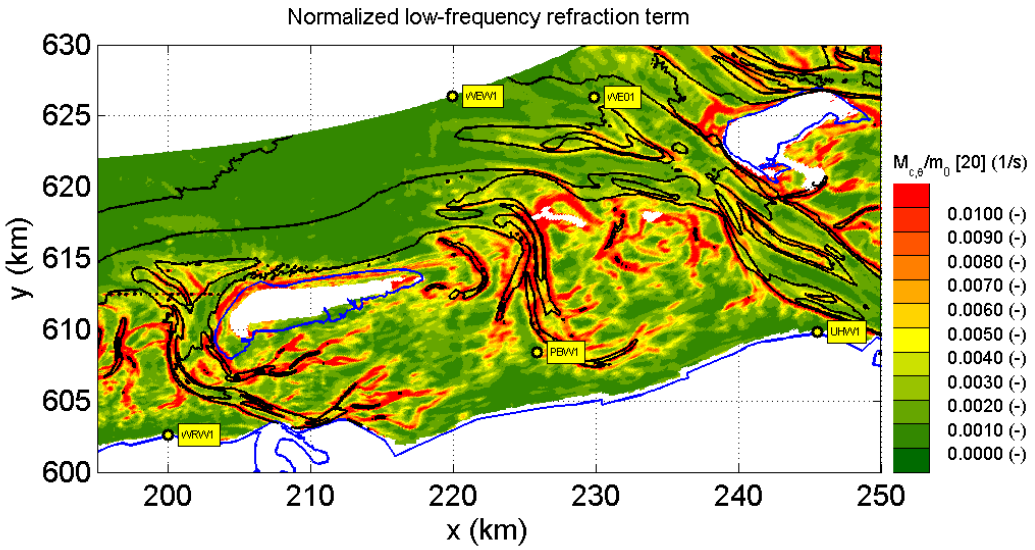

Figure 9: Geographical variation of the normalized magnitude of the refraction term for the frequency range up to 0.2 Hz. Storm instant 9 Nov. 2007, 9:40 hours.

Sensitivity analysis

The results of SWAN hindcast using the default settings (Figure 3) show that especially the low-frequency wave components up to 0.20 Hz are under-predicted. This mismatch can be due to incorrect boundary conditions, such as the water level, or due to incorrect wave model settings or model parameterisations. As discussed earlier, refraction and wave dissipation are significant processes affecting the penetration of low-frequency waves into the interior of the Wadden Sea. We therefore investigated the effects of errors in boundary conditions and possible ways to improve the prediction of the low-frequency components by varying the related settings or model formulations. Here we present results of five variations in wave model set-up:

- Neglecting currents in the input, to determine the effect of currents on the low-frequency wave penetration;
- Increasing the water levels by 0.5 m for the whole computational grid:
- Decreasing the effect of bottom friction by taking the JONSWAP friction factor C_{bfr}=0.038 m^2s^{-3}, equal to the recommended value for swell dominated systems. Support for this choice has been given by Zijlema (2009) who performed SWAN computations for the tidal inlet of Ameland;
- Applying the frequency-squared dependent distribution of surf-breaking dissipation according to Chen et al. (1997). Then the source term for surf breaking can be written as: $S_{brk,2}(f,\theta) = D_{tot}\frac{m_0}{m_2} f^2 \frac{E(f,\theta)}{E_{tot}}$, with D_{tot} the bulk dissipation rate according to Battjes-Janssen (1978) and m_0 and m_2 are the zeroth and second moment of the directionally integrated frequency spectrum $E(f)$;

- Applying a frequency-squared dependent limiter on the refraction term c_θ for frequencies up 0.2 Hz according to $F_{\theta,2} = \begin{cases} (f/0.2)^2 & f \le 0.2 Hz \\ 1 & f > 0.2 Hz \end{cases}$
  In SWAN this is implemented as: $c_\theta^* = F_{\theta,2}\, c_\theta$.

The results of the sensitivity runs are presented in Figure 10 in the form of measured and computed frequency spectra for the default run and for the specific sensitivity runs at the shallow water buoy locations PBW1, UHW1 and WRW1. For brevity, results are only presented for the time instant of the peak water level (i.e., 9 Nov. 2007, 9:40 hours). The water depth, water level, and measured and computed low-frequency parameters H_{20} and T_{20} are also shown in these figures. The default run is coded as (STD). The various alternative model variations (including boundary conditions) are coded as follows: deactivation of currents (NOC), increased water level by 0.5 m (LV05), reduced JONSWAP bottom friction (CF038), limiter on refraction (LFR2), and frequency dependent wave breaking (FBR2).

Deactivating currents only affects the wave spectrum at location PBW1 but not for the other buoys. This difference is probably due to the fact that buoy PBW1 is relatively close to a tidal channel, such that currents affect the propagation of low-frequency waves locally.

Increasing the water level by 0.5 m increases both the low-frequency wave height H_{20} and wave period T_{20} significantly. This sensitivity illustrates the need for accurate water level predictions in shallow areas like the Wadden Sea.

Applying a lower bottom friction, in fact using the JONSWAP coefficient originally derived for swell dominated systems, results in a slight increase in low-frequency wave energy. Energy levels above the peak of the spectrum are not affected due to their greater relative depth. This suggests that in this higher frequency range the energy level is determined by a local balance of wind input, non-linear interactions and whitecapping dissipation.

Applying a limiter on the refraction term c_θ for frequencies lower than 0.2 Hz causes an increase in low-frequency energy levels, whereas the energy levels above the peak frequency are not affected. The most prominent results are found for the nearshore buoys UHW1 and WRW1. For these buoys, the mismatch in low-frequency wave energy is almost halved. Applying the refraction limiter reduces the tendency of the wave to turn towards the banks of the tidal channels, such that they can propagate further into the interior of the Wadden Sea. It is noted that from a theoretical point of view no reason exists to doubt the computation of refraction in the SWAN model. This has been confirmed by numerous verification computations for academic situations. In the present application, the limiter on refraction is applied purely to illustrate this model sensitivity.

The effect of applying a frequency dependent distribution of bulk dissipation causes less low-frequency wave energy to break on the shallow ridges in the ebb tidal delta and on the shallow tidal flats. For buoy PBW1 the effect is rather small, but it is significant for the buoys UHW1 and WRW1. The results also show that the energy levels in the tail of the spectrum are not affected suggesting that in this frequency range a local balance exists. It is noted that using a frequency-dependent distribution of bulk dissipation has, so far, not been applied in spectral modeling of wind waves in shallow water.

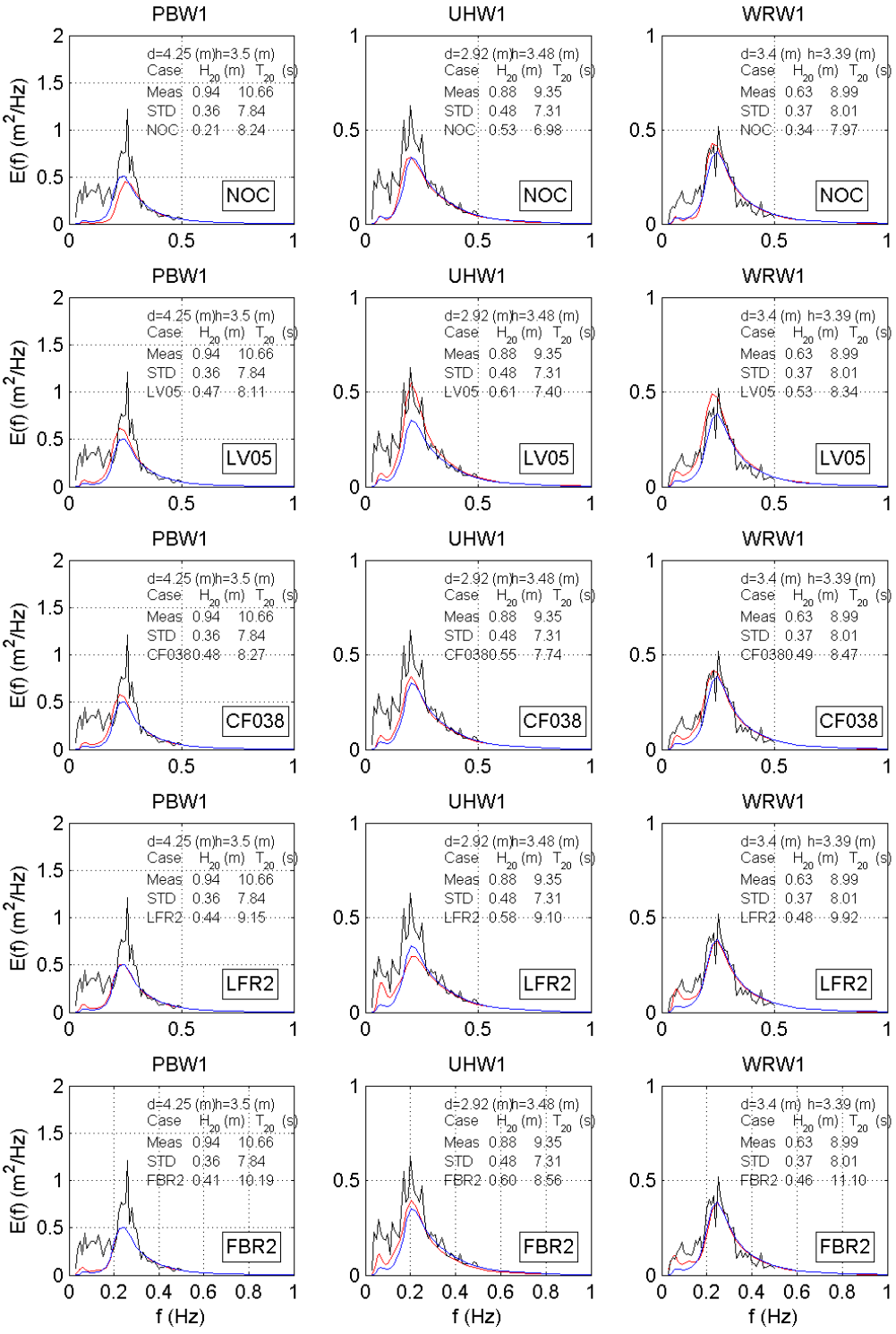

Figure 10: Measured and computed frequency spectra for the buoys PBW1, UHW1 and WRW1 for storm instant 9 Nov. 2007, 9:40 hours. Default SWAN (blue), results of alternative settings (red). Type of variation indicated in rectangular box. Local water depth and water level as well as measured and computed low-frequency parameters H_{20} and T_{20} are tabulated.

Statistical analysis

A regression analysis was performed on the results for all five time instants. The effect of each model variation on the measured and computed low-frequency wave height H_{20} is summarized in Figures 11 and 12. The best fit line according to the model $y=ax$ is shown in red. The line of perfect agreement is given as a black dashed line. Note, that for some buoys no data is available at time instants with too shallow water. Figure 11 shows a comparison of the measured and computed low-frequency wave height H_{20} for the default settings defined here (STD) and the alternative model settings. The results in Figure 11 show that deactivating currents results in slightly poorer estimates of low-frequency wave heights H_{20}, whereas all the other model variations lead to an improvement of the same order. Still, neither of these other formulations removes the under-estimation completely.

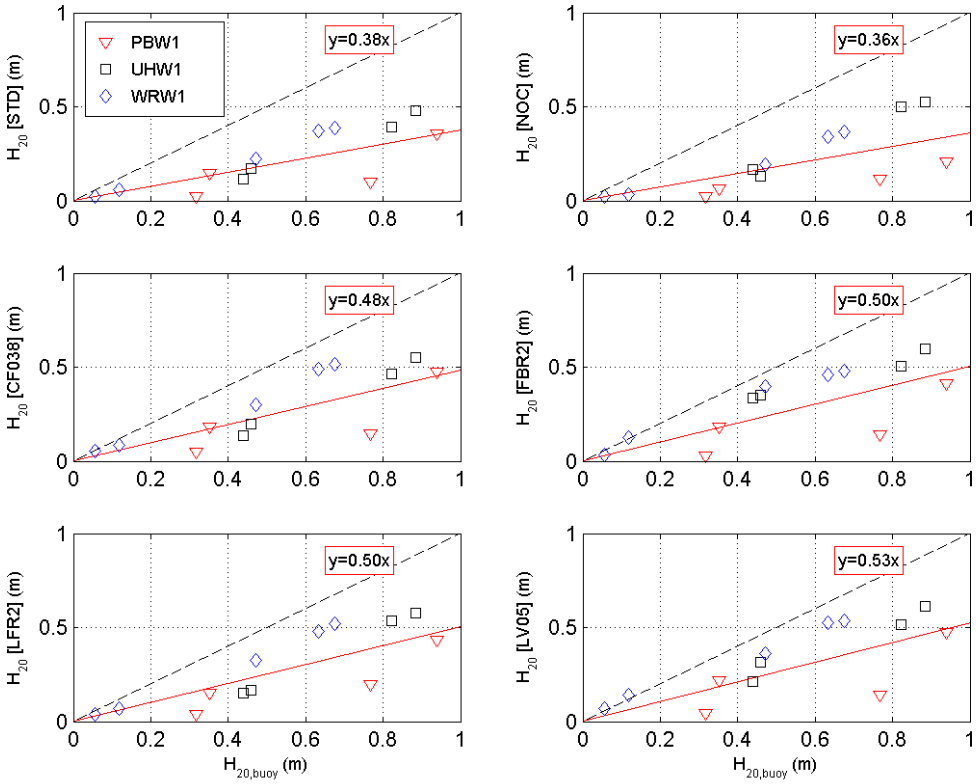

Figure 11: Comparison of measured and computed low-frequency wave heights H_{20} for the default model setting and the five alternative settings. Results are given for 5 storm instants and given for the shallow water buoys PBW1, UHW1 and WRW1. Best fit line (red).

Figure 12 shows a comparison between the computed low-frequency wave heights H_{20} as computed for each alternative model setting compared to the default SWAN setting. The results indicate that the effect of each modification is more or less equal for all buoys and all time instants considered in the sensitivity analysis, except for case with deactivated currents. The results confirm that deactivating currents slightly worsen the results, suggesting that currents hardly play a role in the penetration of low-frequency wave energy towards the shallow water buoy locations. Not shown here, but the effects of current are more noticeable in and near the tidal channels. The effects of reducing bottom friction, frequency dependent dissipation by wave breaking and a limiter on refraction are all of the same order (30%).

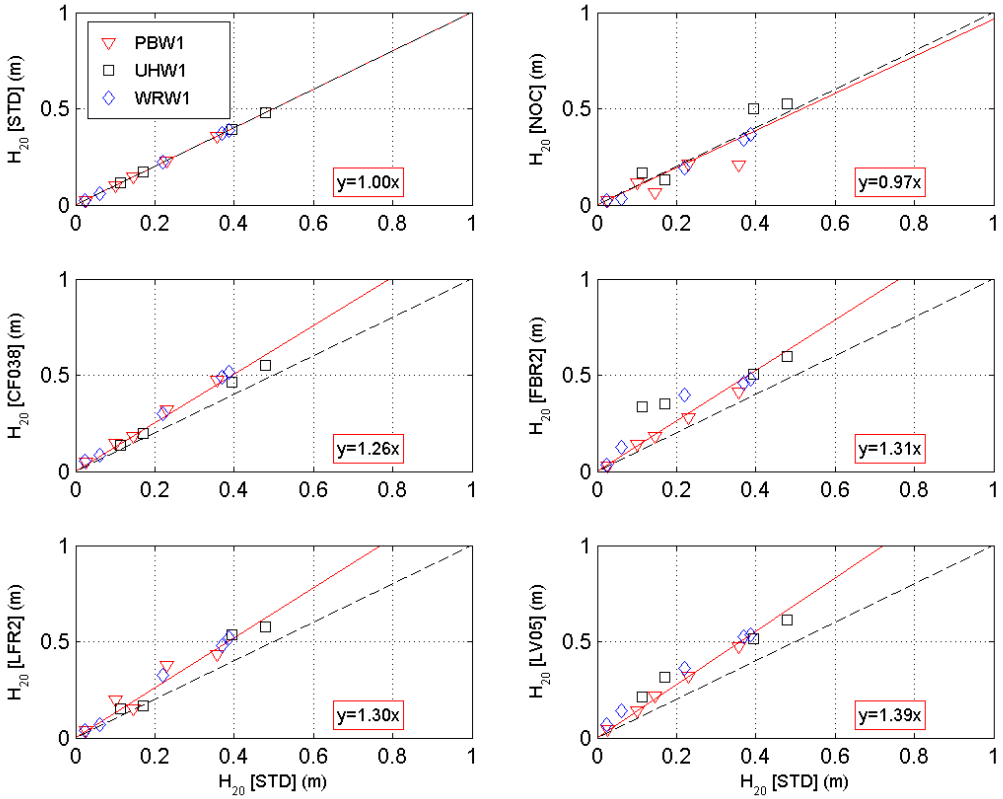

Figure 12: Comparison of computed low-frequency wave heights H_{20} for the default model setting and those obtained for the five alternative settings. Results are given for 5 storm instants and given for the shallow water buoys PBW1, UHW1 and WRW1. Best fit line (red).

Summary

A wave hindcast has been made in the Dutch Eastern Wadden Sea for the severe winter storm of 9 November 2007. Coupled flow-wave model (Delft3D-SWAN) simulations were made to reconstruct the time- and space-varying current and water level fields. The coupled models were driven by spatially uniform but time varying wind fields on the basis of wind measurements at a representative location in the Dutch Eastern Wadden Sea. The forces from the wave model were obtained from the radiation stresses computed with the SWAN model. Computations with the default settings of SWAN version 40.72 (status July 2009) show that SWAN strongly under-predicts wave energy up to 0.20 Hz at the shallow location in the interior of the Wadden Sea. The possible causes of this under-prediction were investigated. Sensitivity runs with alternative model settings, showed that refraction and dissipation effects play a significant role in the penetration of low-frequency wind wave energy. In addition, a small increase in overall water level leads to a significant increase in low-frequency wave energy in the interior of the Wadden Sea and currents hardly affect the amount of low-frequency energy at the shallow water locations.

Conclusions

Based on the coupled flow-wave model runs the following conclusions can be drawn:

- Wave effects contribute significantly to the total water level setup. For the present storm its contribution was about 0.40 m in the eastern Wadden Sea.
- Driving the coupled flow-wave model with measured wind provided more accurate predictions of water levels than using HIRLAM winds.
- Using radiation stresses from the wave model to force the flow model yielded more accurate and more realistic results than using wave dissipation.

Based on the detailed SWAN hindcast and results of the sensitivity analysis the following conclusions can be drawn:

- The default SWAN model under-estimates low-frequency wind wave energy in the interior of the Dutch Eastern Wadden Sea;
- Currents hardly affect the amount of low-frequency wave energy near the shallow water buoys PBW1, UHW1 and WRW1. This finding, however, does not imply that currents can be omitted from a hindcast run, since they do affect the wave fields in and near the tidal channels. In addition, it must be noted that currents were not (yet) measured, thus creating an uncertainty in the interpretation of these results;
- The amount of low-frequency wave penetration is rather sensitive to variations in the water level. Therefore, an accurate prediction of the water levels is important for any wave hindcast in the shallow areas like the Wadden Sea. Evidently, this also holds for the bottom level;
- Refraction and wave dissipation are the dominant processes affecting the penetration of low-frequency wind wave energy in the Wadden Sea;
- Limiting the refraction for low-frequencies causes more low-frequency wave energy to penetrate into the Wadden Sea, as well as applying less bottom friction or using a frequency-dependent distribution of the bulk dissipation of surf breaking;
- Each of the above modifications alone does not remove the under-estimation of low-frequency wave energy completely. Combinations of these, and possible other yet unknown, modifications are needed to remove this under-estimation.

Recommendations

The present work is part of ongoing investigations to improve the SWAN model for applications in the Dutch Eastern Wadden Sea. Based on the work presented here the following recommendations are given:

- From the view point of flow model forcing, more extensive wind measurements or more detailed wind modeling are needed to better resolve the spatial variation of wind fields. In addition, current measurements should be carried out to further improve the flow modelling;
- From the view point of wave model forcing, more wave buoys are needed to resolve the variation of wave characteristics along the northern boundary of the computational grid;
- From the view point of model validation, more wave buoys should be deployed in the interior of the Wadden Sea to track the evolution of the wave field as low-frequency waves propagate into the interior of the Wadden Sea. Another recommendation is to use shore-based remote-sensing techniques to infer two-dimensional wave patterns;
- The effect of using combinations of alternative model settings on the penetration of low-frequency wind wave energy should be investigated;

- The above findings are based on the analysis of only one winter storm. It is therefore strongly advised to verify possible wave model improvements for other storms and areas as well.

Acknowledgement
The presented work is part of the SBW Waddenzee (Strength and Loads and Flood Defenses) project commissioned by Rijkwaterstaat Centre for water Management in the Netherlands.

REFERENCES

Battjes, J.A., and J.P.F.M. Janssen, 1978: Energy loss and set-up due to breaking of random waves, *Proceedings of 14th International Conference on Coastal Engineering*, ASCE, 466-480.

Booij, N., R.C. Ris, and L.H. Holthuijsen, 1999: A third generation wave model for coastal regions, Part I, Model description and validation. *J. Geophys. Res.*, 104, C4, 7649-7666.

Bouws, E., and G.J. Komen, 1983: On the balance between growth and dissipation in an extreme, depth limited wind-sea in the southern North Sea. *J. Phys. Oceanogr.*, Vol. 13, 9 1653-1658.

Chen, Y., R.T. Guza, and S. Elgar, 1997: Modeling of spectra of breaking surface waves in shallow water. *J. of Geophys. Res.*, Vol. 102, C11, 25,035-25,046.

Dingemans, M.W., A.C. Radder and H.J. de Vriend, 1987: Computation of the driving forces of wave-induced currents, *Coastal Engineering,* Vol. 11, 539-563.

Eldeberky, Y., 1996: Nonlinear transformation of wave spectra in the nearshore zone. Ph.D. thesis, Delft University of Technology. Dep. Civil Engineering.

Groeneweg, J., A.J. van der Westhuysen, G.Ph. van Vledder, J.J. Jacobse, J. Lansen and A.R. van Dongeren, 2008: Wave modelling in a tidal inlet: performance of SWAN in the Wadden Sea. *Proc. 31th Int. Conf. on Coastal Engineering*, ASCE, 411-423.

Hasselmann, S., K. Hasselmann, J.H. Allender, and T.P. Barnett, 1985: Computations and parameterisations of the nonlinear energy transfer in a gravity wave spectrum. Part II: parameterisations of the nonlinear transfer for application in wave models. J. *Phys. Oceanogr.*, 15, 11, 1378-1391.

Holthuijsen, L.H., M. Zijlema, and P.J. van der Ham, 2008: Wave physics in a tidal inlet. *Proc. 31th Int. Conf. Coastal Engineering*, ASCE, 437-448.

Kaiser, R. en H.D. Niemeyer. 2001. Analysis of directional spectra in shallow environment. *Proceedings of 4th international symposium WAVES*, 944-952.

Van der Westhuysen, A.J., M. Zijlema, and J.A. Battjes, 2007: Nonlinear saturation–based whitecapping dissipation in SWAN for deep and shallow water. *Coastal Engineering*, Vol. 54, 151-170.

Van Vledder, G.Ph., J. Groeneweg, A.J. van der Westhuysen, and A.R. van Dongeren, 2007: Numerical aspects and source term analysis of wave modeling in a tidal inlet. *Proc. 10th workshop on Wave Hindcasting and Forecasting*, North Shore, Oahu, Hawaii, USA.

Van Vledder, G.Ph., J. Groeneweg, and A.J. van der Westhuysen, 2008: Numerical and physical aspects of wave modelling in a tidal inlet. *Proc. 31th Int. Conf. on Coastal Engineering*, ASCE, 424-436.

WL|Delft Hydraulics, 2004: Golfstatistiek op relatief diep water 1979-2002 (Wave statistics at relatively deep water 1979-2002), Appendix I to report Q3770.

Yan, L., 1987: An improved wind input source term for third generation ocean wave modelling. Technical Report, No. 87-8. Royal Dutch Meteor, Inst.

Zijderveld, A. and H. Peters, 2008: Measurement program Ducth Wadden Sea. *Proc. 31th Int. Conf. Coastal Engineering,* ASCE, 404-410.

Zijlema, M., 2009: Multiscale simulations using unstructured mesh SWAN model for wave hindcasting in the Dutch Wadden Sea. *Proc. Coastal Dynamics 2009*, paper 2.